A Fast On-Board Integrated Battery Charger for EVs Using an Asymmetrical Six-Phase Machine

I. Subotic, E. Levi, N. Bodo
Liverpool John Moores University
School of Engineering, Technology and Maritime Operations
Liverpool L3 3AF, U.K.
i.subotic@2011.ljmu.ac.uk, e.levi@ljmu.ac.uk, n.bodo@2009.ljmu.ac.uk

***Abstract*–The paper considers a novel fast charging topology for electric vehicles (EVs). Instead of being made as a separate unit, the proposed on-board charger utilizes power electronics components that already exist inside the vehicle, namely an asymmetrical six-phase propulsion motor and a six-phase inverter. The charger can operate at unity power factor, and is capable of vehicle-to-grid (V2G) operation as well. Additional degrees of freedom of the six-phase machine are employed in order to transfer a part of excitation from the torque producing to non-torque/flux producing plane of the machine. Consequently, electromagnetic torque is not produced in the machine during the charging/V2G process, so that the rotor does not have to be mechanically locked. A theoretical analysis of the operating principles is reported, and simulation results are given for both charging and V2G mode of operation.**

Keywords–battery chargers; electric vehicles; integrated on-board chargers; multiphase machines.

I. INTRODUCTION

Nowadays, two types of battery chargers for EVs are used: fast off-board dc chargers and slow on-board ac chargers. Although the former have a great advantage that they can charge a battery in up to 15 minutes, their drawback is that the drivers have to search for charging stations that are sparsely distributed, and plan their route according to their disposition. On the other hand, on-board chargers provide certain flexibility to charging, since ac mains are widely available. However, on-board chargers are typically only capable of slow charging, since they rely on utilization of the single-phase grid.

It has to be noted that, during the charging process, the most of the elements of EVs that have a function in the propulsion mode, e.g. an inverter and a propulsion motor, are idle. The idea of reusing some of these elements for the charging mode has been introduced more than thirty years ago [1]. By reusing the existing components, fewer new components are required to be placed on-board, and consequently savings in cost, weight and spare space are made. These advantages of integrated chargers have made the topic an interesting area for research. Numerous proposals for integration have been made until now [2], mostly for single-phase (slow) charging.

The preferred types of propulsion machines in EVs are induction and permanent magnet machines [3]. However, only a few configurations capable of fast charging incorporating these types of machines have been reported [4-12]. Moreover, most solutions require mechanical locking of the machine's rotor, since a torque gets developed in the machine during the charging mode, leading to low efficiency, increased wear and noise. Only five of the configurations [8-12] allow three-phase (fast) charging without a torque production in the machine.

A configuration which in propulsion mode consists of a three-phase machine in an open-winging configuration, supplied from a triple H-bridge inverter, is considered for integration into the charging process in [8]. In the charging mode grid is connected to the mid-points of the machine's phase windings. By simultaneous switching of converter legs connected to the same grid phase, equal spreading of the grid phase current through each two half-windings in spatial opposition is achieved. Since these half-windings cancel each other's effect, there is no rotating field production in the rotor. However, the machine has to be custom made in order to allow access to the phase windings' mid-points (in essence, the machine has to be a symmetrical six-phase machine). The configuration has an advantage that it does not require any hardware reconfiguration between the charging and propulsion mode and it is currently considered for use in future electric vehicles by Valeo [13].

A configuration with the same advantages as the previous one, but based on utilization of a nine-phase machine with three isolated neutral points, is presented in [9]. In the charging mode three-phase grid is directly connected to the three isolated neutral points of the machine. By using proper converter control, it is ensured that the same currents flow through all three machine's phases that are connected to the same grid phase, thus cancelling each other's effect. There is again no field production in the rotor, and no need for any hardware reconfiguration between the operating modes.

Renault ZOE is the first commercial vehicle that employs an integrated fast charger [10]. In addition to the integrated elements, which are the inverter and a three-phase propulsion motor, the charger requires a junction box. It manages the charging process, converts the ac current into dc current (thus requiring additional power electronics) and communicates with the charging station. The charging process is without torque production. However, total converter installed power is increased due to the addition of the charging rectifier.

The authors would like to acknowledge the Engineering and Physical Sciences Research Council (EPSRC) for supporting the Vehicle Electrical Systems Integration (VESI) project (EP/I038543/1).

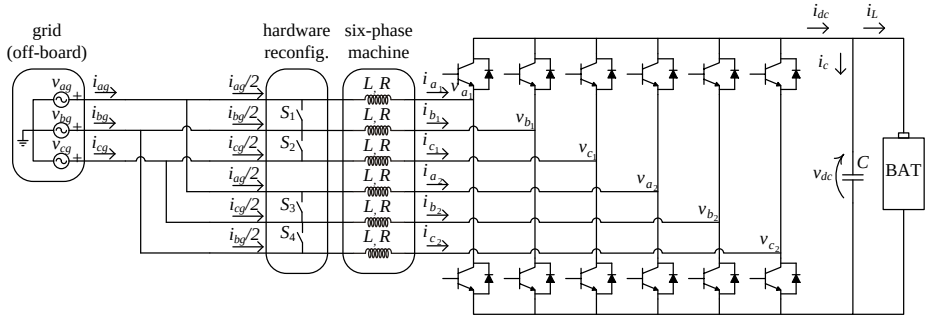

Fig. 1. Topology of the asymmetrical six-phase integrated fast battery charging system.

Configurations with a symmetrical and an asymmetrical six-phase machine were considered in [11]-[12]. They employ the principle of phase transposition [14] in order to avoid torque production during the charging mode. However, they require a transformer with dual secondary, which is a non-integrated element, to realise the six-phase supply.

A novel charger, employing an asymmetrical six-phase machine, is proposed in this paper. It has a distinct advantage over the one introduced in [12] since it does not require a transformer. Hence it connects to the three-phase supply directly and can be entirely integrated on-board the vehicle.

The paper is organised as follows. In section II a theoretical analysis of the proposed configuration is performed. Section III provides a control algorithm for the charging/V2G mode. In section IV simulations are performed for both charging and V2G mode of operation in order to validate the theoretical results. Section V outlines conclusions of the paper.

II. Operating Principles of the Proposed Charging System

The considered topology is shown in Fig. 1. In the propulsion mode switches S_1-S_4 are closed, the six-phase machine has two isolated neutral points, and mains are disconnected. For the charging mode the topology requires reconfiguration. The switches have to be opened, leaving the machine in an open-end winding (OeW) configuration. The three-phase grid is connected to the machine terminals as follows. The connection to the first set of machine windings follows the phase order of the machine. (i.e. a_g-a_1, b_g-b_1 and c_g-c_1). However, the order of connections to the second set differs from the phase order of the machine's windings. Grid phases a_g, b_g and c_g are now connected to machine phases a_2, c_2 and b_2 respectively (Fig. 1).

During the charging process, when three-phase currents flow through the set of three-phase machine windings, the set develops a rotating field. However, by using the specific order of grid connections to the second set, it is achieved that the second set produces a rotating field that rotates in the opposite direction compared to the one produced by the first set (Fig. 2). Since the speed and magnitude of these rotating fields are the same, the overall resultant field is pulsating, and hence not capable of producing an average torque; thus the rotor does not have to be mechanically locked.

Machine's behaviour in the charging mode can be assessed by examining the 2D space vectors of the asymmetrical six-phase system [15]. These can be formulated as (f stands for any variable that is transformed, e.g. voltage, current, etc.):

$$\begin{aligned} \underline{f}_{\alpha\beta} &= \sqrt{2/6}\left(f_{a_1} + \underline{a}^4 f_{b_1} + \underline{a}^8 f_{c_1} + \underline{a} f_{a_2} + \underline{a}^5 f_{b_2} + \underline{a}^9 f_{c_2}\right) \\ \underline{f}_{xy} &= \sqrt{2/6}\left(f_{a_1} + \underline{a}^8 f_{b_1} + \underline{a}^{16} f_{c_1} + \underline{a}^5 f_{a_2} + \underline{a} f_{b_2} + \underline{a}^9 f_{c_2}\right) \end{aligned} \quad (1)$$

where $\underline{a} = \exp(j\delta) = \cos\delta + j\sin\delta$ and $\delta = \pi/6$. The grid currents can be given as

$$i_{kg} = \sqrt{2} I \cos(\omega t - l\,2\pi/3) \qquad l = 0,1,2 \qquad k = a,b,c \quad (2)$$

The relationship between machine and grid phase currents is, according to Fig. 1, given with

$$i_{a_1} = i_{a_2} = \frac{i_{ag}}{2}; \quad i_{b_1} = i_{c_2} = \frac{i_{bg}}{2}; \quad i_{c_1} = i_{b_2} = \frac{i_{cg}}{2} \quad (3)$$

By substituting (2) and (3) into (1), the following two space vectors are obtained:

$$\begin{aligned} \underline{i}_{\alpha\beta} &= \sqrt{3/8} \cdot I\,(\exp(j\omega t) + \exp(-j\omega t) \cdot \exp(j\pi/6)) \\ &= \sqrt{3/2}\, I \cos(\omega t - \pi/12) \cdot (0.966 + j \cdot 0.259) \end{aligned} \quad (4)$$

$$\begin{aligned} \underline{i}_{xy} &= \sqrt{3/8} \cdot I\,(\exp(j\omega t) \cdot \exp(j5\pi/6) + \exp(-j\omega t)) \\ &= \sqrt{3/2}\, I \cos(\omega t + 5\pi/12) \cdot (0.259 + j\,0.966) \end{aligned} \quad (5)$$

Zero-sequence components are both equal to zero.

It can be seen from (4) that the β-component is 3.73 times smaller than the α-component. Since these two components are proportional they form a straight line if represented in the complex plane. The graphical representation of equation (4) is given in Fig. 3. As can be seen, the excitation in the torque producing (α-β) plane is pulsating, since a part of the excitation is transferred into the non-torque producing (x-y) plane (5). The excitation that is left in α-β plane is not capable of producing a starting torque in the machine; thus the rotor stays at standstill during the charging process.

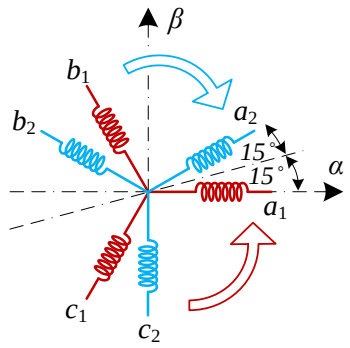

Fig. 2. Spatial representation of the two winding sets and their rotating fields.

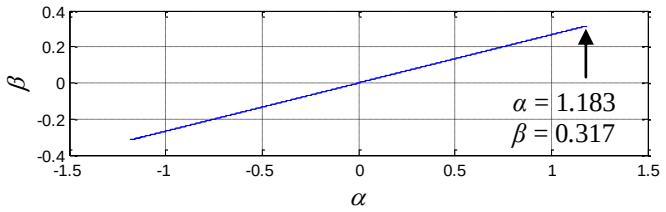

Fig. 3. Graphical representation of (4).

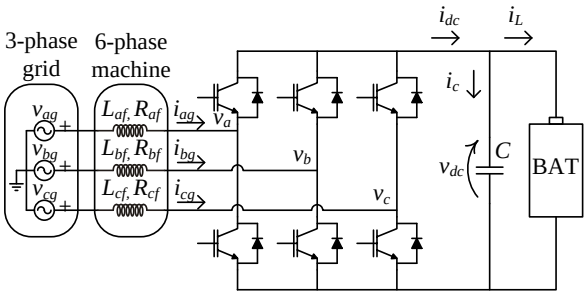

Fig. 4. Equivalent scheme of Fig. 1 for the charging/V2G mode of operation.

III. Control Algorithm for the Charging/V2G Mode of Operation

It was shown in the previous section that the machine will stay at standstill during the charging process. Since the torque is not produced, the rest of the system sees the machine as a passive network, consisting of a resistance and an inductance in each phase. Pairs of phases are controlled in parallel, thus the same currents flow through two phases that make a pair (e.g. a_1-a_2, see Fig. 1), and each pair can be represented with an equivalent resistive-inductive circuit and an inverter leg. Machine phases a_1-a_2 are represented with L_{af}, R_{af}, phases b_1-c_2 with L_{bf}, R_{bf}, and c_1-b_2 with L_{cf}, R_{cf}. The resulting equivalent scheme for the charging/V2G process is given in Fig. 4, and it can be seen that this configuration corresponds to a standard three-phase voltage source converter.

In order to comply with grid regulations, near unity power factor has to be achieved. Hence, the grid voltage oriented control (VOC) is utilized for controlling the configuration of Fig. 4. The control algorithm is given in Fig. 5.

At first, the grid voltage position has to be determined. In order to achieve this, grid voltages have to be measured, and the position determined by phase-locked loop (PLL). Once the information on grid position is obtained, it is used to transform

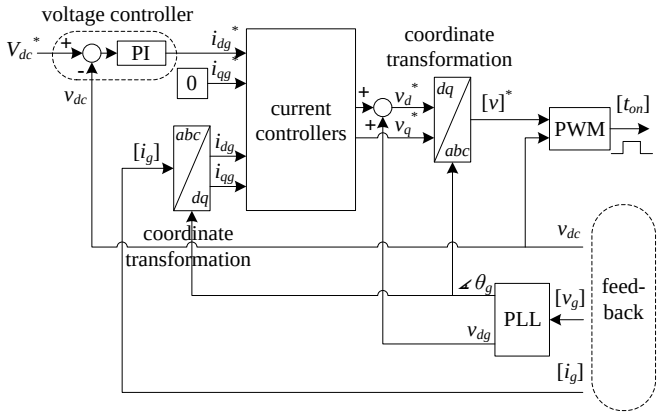

Fig. 5. Grid VOC algorithm for the charging mode of operation.

grid currents into the reference frame that is grid voltage oriented. In this reference frame current components appear as dc quantities. However, the components that are in phase and out of phase with grid voltage are separated. The *d*-component is in phase with the grid voltage and this component can be used for energy transfer. The *q*-component is out of phase with the voltage; thus it should be controlled to zero in order to achieve unity power factor. Since both components are dc quantities, they can be controlled with PI controllers.

The charging process consists of two modes: constant current (CC) and constant voltage (CV) mode. In CC mode the battery is charged with a constant current, and the reference for *d*-current component is a constant. In CV mode the voltage that is applied to the battery is constant and the reference for the *d*-current component is the output of a voltage controller. The voltage controller is shown in Fig. 5 as the outer control loop.

Current controllers are presented in Fig. 6. As can be seen, PI controllers control the *d*- and *q*-components as in a standard voltage source rectifier. However, since the three pairs of *R-L* parameters of Fig. 4 are not mutually equal, they introduce asymmetry into the system. The reason for the asymmetry is that the field in the machine is pulsating during the charging process. The field from rotor causes different induced voltages in different phases, since they are spatially shifted by different angles from the direction of the pulsating field (e.g. phase a_1 by 15˚, b_1 by 105˚, c_1 by 225˚). Thus the equivalent per-phase *R-L* parameters of Fig. 4 contain unequal portions of rotor leakage inductance and resistance.

The asymmetry is reflected through the second harmonic in the *d-q* reference frame. The harmonic rotates in anti-synchronous direction. One way of achieving symmetrical currents is to transform the second harmonic (as seen from the *d-q* reference frame) into a reference frame in which it is seen as a dc quantity, and then to control it by a PI controller. The reference frame has to rotate two times faster than the synchronous speed in the opposite direction. The additional controller that is used for asymmetry control is depicted in the lower part of Fig. 6.

The outputs of current controllers are reference voltage signals for the inverter. A simple carrier-based PWM with the zero-sequence injection is used as the modulation strategy.

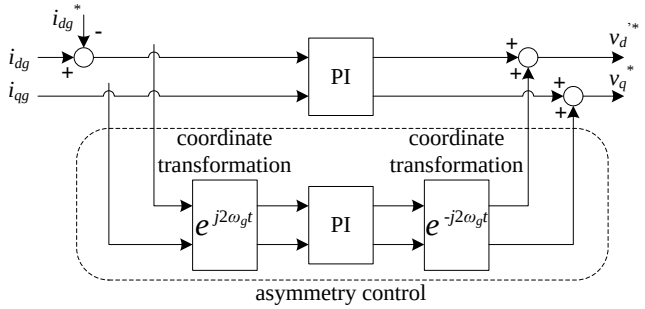

Fig. 6. Current controllers.

Although V2G is a different mode of operation, the control differs insignificantly from the charging mode. The algorithm of Fig. 5 is still valid. The only difference is that the reference for the *d*- current component is a constant with a negative value. The *q*-component should be again controlled to zero. Currents are then in phase opposition with the grid voltages, and unity power factor is achieved.

For the propulsion mode switches S_1-S_4 have to be closed, and the machine operates with two isolated neutral points according to the field oriented control (FOC) principles. This mode of operation is well known for asymmetrical six-phase machines and will not be considered here.

IV. Simulation Results

Matlab/Simulink simulation results of the proposed fast charger are presented in this section, for both charging and V2G modes of operation. The three-phase grid is taken as perfectly sinusoidal with phase voltage of 240V_{rms} and 50Hz frequency. The switching frequency of the converter is 10kHz, and the dead-time effect is neglected. The dc-bus capacitance is taken as 1.5mF. Battery is modelled with an ideal voltage source E in series with a resistor R_L=0.5Ω, which represents battery's internal resistance. Asymmetrical six-phase induction machine parameters, used in the simulation, are the following: R_s =12.5 Ω, R_r = 6Ω, L_{ys} =5.5mH, L_{yr} = 11mH, L_m = 590mH, three pole pairs, J = 0.1kgm^2. The charging mode is considered first.

A. Charging Mode

For this mode of operation the reference for the dc-bus voltage is set to 600V, and the ideal voltage source of the battery is taken as E = 597V. It should be noted that this value does not have to be the same for all modes of operation. In fact it is quite common that EVs have a dc-dc converter between the battery and the dc-bus capacitor, so that various values can be achieved. In the next subsection a different value is considered for E.

Fig. 7a illustrates the grid currents. Although the machine's equivalent *R*-*L* parameters in Fig. 4 are different for each grid phase, the currents are symmetrical due to the added asymmetry control (the lower part of Fig. 6). However, it can be seen that the phase *a* has the smallest current ripple among the three phases. The rotor winding's influence is the most prominent in this phase since it is spatially shifted by the smallest angle (±15˚) form the rotor's pulsating field. The

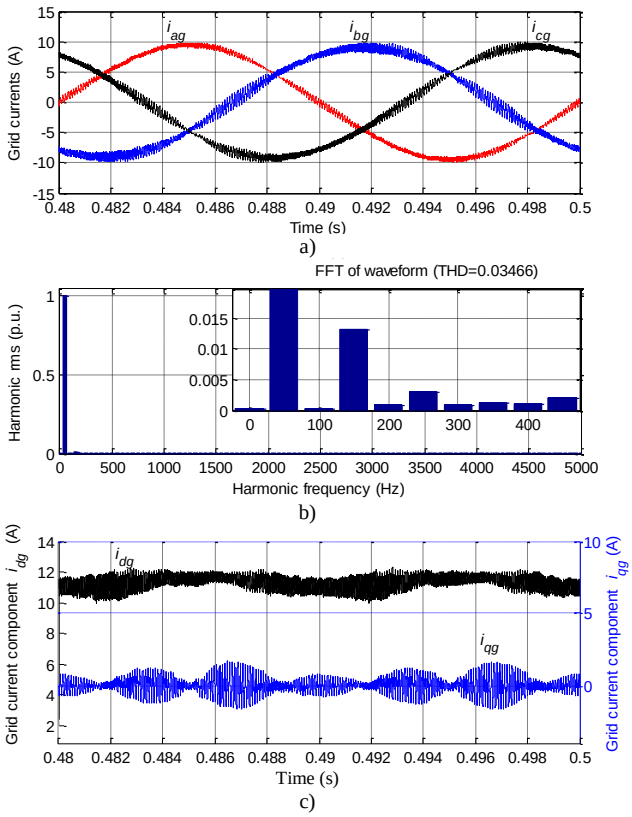

Fig. 7. Charging mode: (a) Grid phase currents, (b) spectrum of grid phase current i_{ag}, (c) grid current components.

effect is amplified by the fact that rotor leakage inductance is two times higher than the stator's in this machine.

The spectrum of the phase *a* current is given in Fig. 7b. It contains only small low order harmonics. The third harmonic (1.3%) is introduced by a pulsating output of the dc-bus voltage controller, as will be shown later. Grid current components are shown in Fig. 7c. The *q*- current component is kept at zero, which shows that the charging is with the unity power factor. The complete energy transfer is achieved by the *d*-component, which is the grid current component that is in phase with the grid voltage. The grid phase voltage and machine phase current i_{a1} are shown in Fig. 8a. It is again obvious that the charging process is with the unity power factor. The machine's i_{a1} current is exactly two times smaller than the grid current i_{ag} at all times. Machine current components are given in Fig. 9. The first (α-β) plane is excited. However, the α and β components have the same phase, thus producing a pulsating field in the machine. Since a pulsating field cannot provide an average torque to start the machine, it stays at standstill. Current components in the non-torque producing plane are shown in Fig. 9b. The excitations in both planes are in accordance with theoretical results given with (4) and (5).

Converter phase voltage and spectrum are given in Fig. 10. Since the dead-time effect is neglected, the spectrum contains only very small low-order harmonics. The machine's torque and speed during the charging process are shown in Fig. 11a. It is obvious that zero torque results during the whole charging

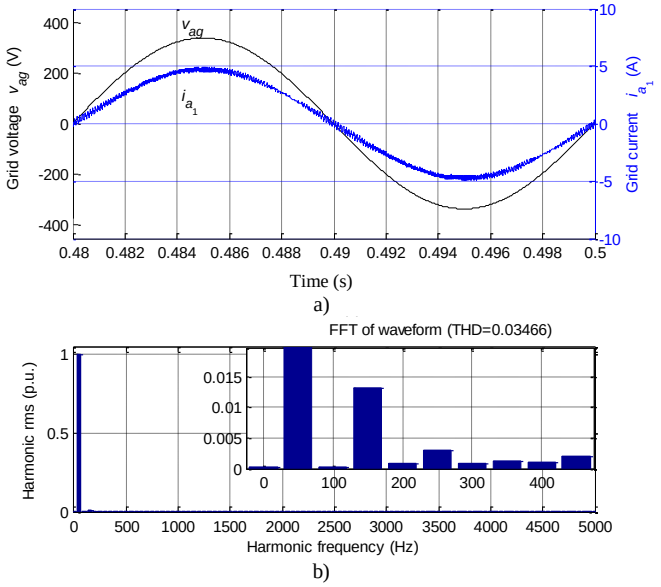

Fig. 8. (a) Grid phase voltage and machine phase current i_{a1} , (b) spectrum of machine phase current i_{a1}.

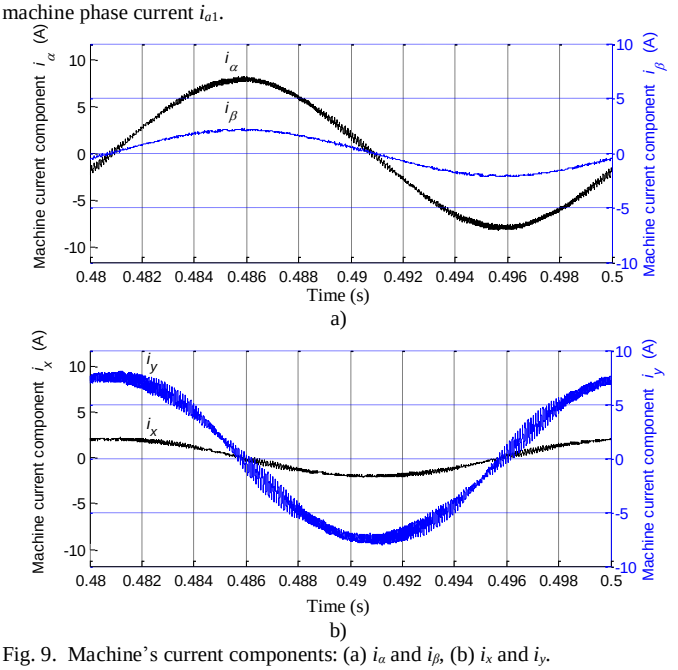

Fig. 9. Machine's current components: (a) i_α and i_β, (b) i_x and i_y.

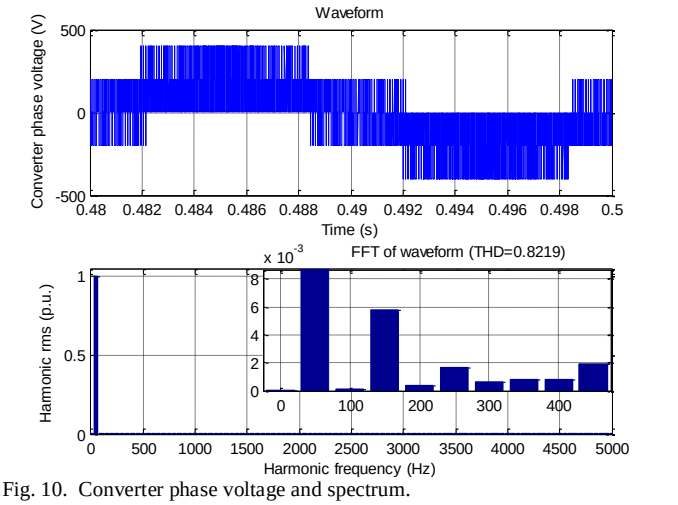

Fig. 10. Converter phase voltage and spectrum.

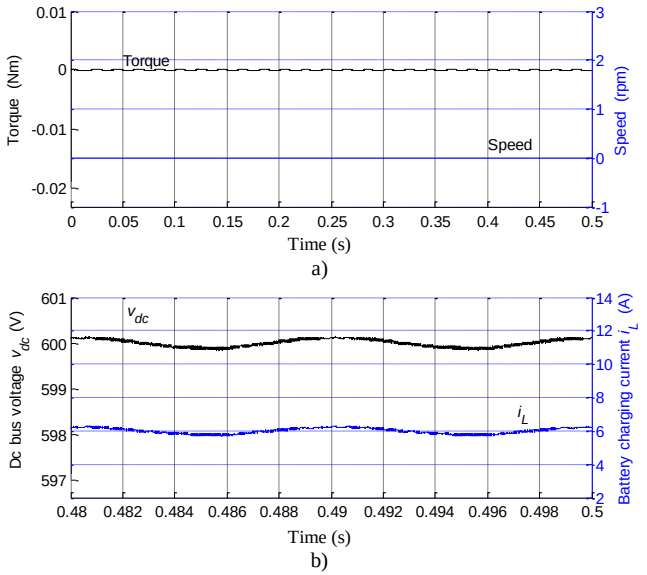

Fig. 11. (a) Machine's torque and speed, (b) dc-bus voltage and battery charging current.

process, and the speed is consequently kept at zero.

The dc-bus voltage and battery charging current are shown in Fig. 11b. The average value of the dc-bus voltage follows the reference without any steady-state error. However, a slight pulsation around the reference is evident. The pulsation is caused by time-dependant losses in the machine. The machine equivalent scheme has different parameters in different phases and, since symmetrical currents flow through these phases, the complete losses are the greatest when the current in the phase with the highest impedance (phase *a*) is at its peak. Considering the fixed power drawn from the grid, the useful energy after the losses is also slightly pulsating. The battery charging current follows the shape of the voltage and has an average value of 6A.

Since the dc-bus voltage is pulsating, the voltage controller tries to compensate this and gives a slightly pulsating reference for the *d*- current component. This manifests itself with a small third harmonic in the current spectrum (Fig. 7b). It should be noted that this harmonic is different in different grid phases, with the sum being always equal to zero.

B. V2G Mode

V2G mode of operation is examined in this subsection. A different value for the ideal voltage source of the battery, E = 753V, is now considered, as explained in the previous subsection. The reference for the dc-bus voltage is set to 750V.

Grid currents, phase *a* current spectrum, and current components are given in Fig. 12. The same conclusions as for the charging mode are valid. However, it can be seen that the *d*-component now has a negative value, which demonstrates that the grid current is in phase opposition with the grid voltage. The absolute value for this current component is smaller than during the charging mode (Fig. 7c) since the power that is injected into the grid is now what is left from the battery discharging power after the filter (i.e. machine) losses.

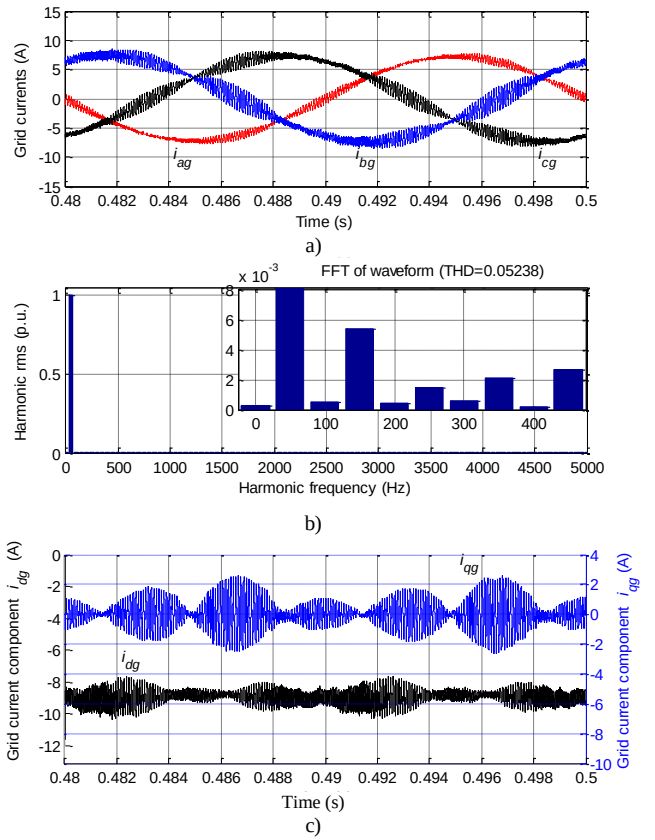

Fig. 12. V2G mode: (a) Grid phase currents, (b) spectrum of grid phase current i_{ag}, (c) grid current components.

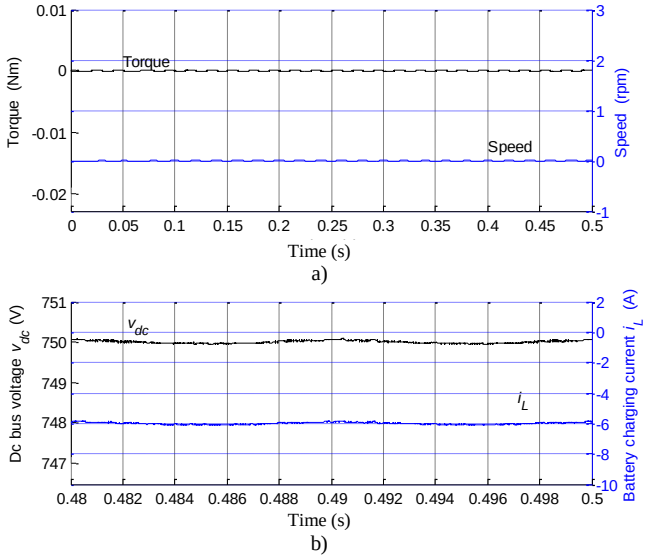

Fig. 13. (a) Machine's torque and speed, (b) dc-bus voltage and battery charging current.

Fig. 13a shows that the average torque and speed are again kept at zero during the whole process; thus the rotor does not have to be mechanically locked during this mode of operation either. The dc-bus voltage is controlled at 750V without any steady-state error (Fig. 13b), and the charging current follows the shape of the voltage. However, the current now has the opposite sign compared to Fig. 11b, demonstrating the battery discharging.

V. CONCLUSION

A novel fast charger for EVs is proposed in the paper. The charging is from a standard three-phase grid, and the charger is completely integrated on-board. Asymmetrical six-phase machine with two isolated neutral points and a six-phase inverter are incorporated into the charging process, avoiding the cost of additional power electronics components. Simulations with a full asymmetrical six-phase machine model are performed for both charging and V2G modes of operation in order to validate the theoretical results and ascertain the torque-free operation.

REFERENCES

[1] J.M. Slicker, "Pulse width modulation inverter with battery charger," *US Patent* 4,491,768, 1985.

[2] S. Haghbin, S. Lundmark, M. Alakula, and O. Carlson, "Grid-connected integrated battery chargers in vehicle applications: review and new solution," *IEEE Trans. on Industrial Electronics*, vol. 60, no. 2, pp. 459-473, 2013.

[3] J. de Santiago, H. Bernhoff, B. Ekergård, S. Eriksson, S. Ferhatovic, R. Waters, and M. Leijon, "Electrical motor drivelines in commercial all-electric vehicles: A review," *IEEE Trans. on Vehicular Technology*, vol. 61, no. 2, pp. 475-484, 2012.

[4] S. Kinoshita, "Electric system of electric vehicle," *US Patent* No. 5,629,603, 1997.

[5] F. Lacressonniere and B. Cassoret, "Converter used as a battery charger and a motor speed controller in an industrial truck," *Proc. Eur. Conf. on Power Electr. and Applications EPE*, Dresden, Germany, CD-ROM paper 0159, 2005.

[6] S. Haghbin, S. Lundmark, M. Alakula, and O. Carlson, "An isolated high-power integrated charger in electrified-vehicle applications," *IEEE Trans. on Vehicular Technology*, vol. 60, no. 9, pp. 4115-4126, 2011.

[7] I. Subotic, E. Levi, M. Jones, and D. Graovac, "Multiphase integrated on-board battery chargers for electrical vehicles," *Proc. European Power Electronics and Applications Conf. EPE*, Lille, France, CD-ROM paper 0304, 2013.

[8] L. De Sousa, B. Silvestre, and B. Bouchez, "A combined multiphase electric drive and fast battery charger for electric vehicles," *Proc. IEEE Vehicle Power and Propulsion Conference VPPC*, Lille, France, CD-ROM, 2010.

[9] I. Subotic, E. Levi, M. Jones, and D. Graovac, "On-board integrated battery chargers for electric vehicles using nine-phase machines," *IEEE Int. Electric Machines and Drives Conf. IEMDC*, Chicago, IL, pp. 239-246, 2013.

[10] Renault press kit, "Renault ZOE: the electric supermini for everyday use," www.media.renault.com, February 26, 2013.

[11] I. Subotic and E. Levi, "An integrated battery charger for EVs based on a symmetrical six-phase machine," *IEEE International Symposium on Industrial Electronics ISIE*, Istanbul, Turkey, 2014, in press.

[12] I. Subotic, E. Levi, M. Jones, and D. Graovac, "An integrated battery charger for EVs based on an asymmetrical six-phase machine," *IEEE Industrial Electronics Society Conf. IECON*, Vienna, Austria, pp. 7242-7247, 2013

[13] A. P. Sandulescu, F. Meinguet, X. Kestelyn, E. Semail, and A. Bruyere, "Flux-weakening operation of open-end winding drive integrating a cost-effective high-power charger", *IET Electrical Systems in Transportation*, vol. 3, no. 1, pp. 10-21, 2013.

[14] E. Levi, M. Jones, S.N. Vukosavic, and H.A. Toliyat, "A novel concept of a multiphase, multimotor vector controlled drive system supplied from a single voltage source inverter," *IEEE Trans. on Power Electronics*, vol. 19, no. 2, pp. 320- 335, 2004.

[15] E. Levi, R. Bojoi, F. Profumo, H.A. Toliyat, and S. Williamson, "Multiphase induction motor drives - a technology status review," *IET Electric Power Applications*, vol. 1, no. 4, pp. 489-516, 2007.